

THE CURSE AND BLESSING OF MEAN BIAS IN FP4-QUANTIZED LLM TRAINING

Hengjie Cao^{1*} Zhendong Huang^{1*} Mengyi Chen¹ Yifeng Yang¹ Fanqi Yu¹
 Ruijun Huang¹ Fang Dong¹ Xin Zhang¹ Jixian Zhou¹ Anrui Chen¹
 Mingzhi Dong² Yujiang Wang^{4,5} Jinlong Hou³ Qin Lv⁶ Yuan Cheng³
 Tun Lu¹ Fan Yang¹ Li Shang¹

¹ Fudan University ² University of Bath ³ Shanghai Innovation Institute
⁴ University of Oxford ⁵ Oxford Suzhou Centre for Advanced Research
⁶ University of Colorado Boulder

ABSTRACT

Large language models trained on natural language exhibit pronounced anisotropy: a small number of directions concentrate disproportionate energy, while the remaining dimensions form a broad semantic tail. In low-bit training regimes, this geometry becomes numerically unstable. Because blockwise quantization scales are determined by extreme elementwise magnitudes, dominant directions stretch the dynamic range, compressing long-tail semantic variation into narrow numerical bins. We show that this instability is primarily driven by a coherent rank-one mean bias, which constitutes the dominant component of spectral anisotropy in LLM representations. This mean component emerges systematically across layers and training stages and accounts for the majority of extreme activation magnitudes, making it the principal driver of dynamic-range inflation under low precision. Crucially, because the dominant instability is rank-one, it can be eliminated through a simple source-level mean-subtraction operation. This bias-centric conditioning recovers most of the stability benefits of SVD-based spectral methods while requiring only reduction operations and standard quantization kernels. Empirical results on FP4 (W4A4G4) training show that mean removal substantially narrows the loss gap to BF16 and restores downstream performance, providing a hardware-efficient path to stable low-bit LLM training.

1 INTRODUCTION

Large language models are trained on massive human language corpora, which induce a characteristic geometry in learned representations. Across layers and training stages, activations exhibit pronounced anisotropy: a small number of directions concentrate disproportionate energy (strong spectral spikes), while the remaining directions form a broad semantic tail (Ethayarajh, 2019; Mu & Viswanath, 2018; Timkey & van Schijndel, 2021; Kovaleva et al., 2021; Machina et al., 2024).

While linguistically natural, this structure becomes a numerical liability under low-bit training. In blockwise quantization, scaling factors are determined by extreme elementwise magnitudes. When a small set of directions dominates the activation spectrum, these extremes stretch the dynamic range, compressing long-tail semantic variation into narrow numerical bins and degrading training stability (Xiao et al., 2023; Frantar et al., 2023; Lin et al., 2024; Li et al., 2024; Ashkboos et al., 2024). Prior mitigation strategies therefore rely on explicit spectral control, often via singular value decomposition (SVD) or orthogonalization procedures, as in Metis (Cao et al., 2025) and related approaches. Although effective, such techniques are computationally intensive, memory-expensive, and poorly aligned with modern accelerator hardware.

In this work, we examine the internal structure of anisotropy and uncover a sharper structural principle: activation anisotropy in LLM training is predominantly driven by a coherent rank-one mean bias.

*Co-first authors.

This mean component is not incidental. At every representational level—tokens, phrases, clauses, and full sentences—language contains shared contextual signal. Self-attention, non-odd nonlinearities, and residual accumulation integrate these shared components across tokens and layers, systematically regenerating and amplifying coherent mean directions in representation space.

Due to high dimensionality, even modest coordinate-wise bias produces substantial vector magnitude. In hidden dimension H , the norm of a coherent mean scales as $\|\mu\|_2 \sim \sqrt{H} \bar{\mu}$, magnifying small per-coordinate drift into dominant elementwise extremes. We show both theoretically and empirically that this rank-one mean component accounts for the majority of extreme activation magnitudes across layers and training stages. Since low-bit quantization scales are governed by these extremes, mean bias becomes the primary driver of dynamic-range inflation and numerical instability.

Crucially, because the dominant instability is rank-one, it admits a simple remedy. A single source-level mean-subtraction operation isolates and removes the coherent bias component before quantization. This operation requires only reduction and elementwise kernels, avoiding costly spectral decompositions while recovering most of their stability benefits. In this sense, the same structure that creates low-bit instability also exposes a low-dimensional handle for efficient mitigation: the blessing of mean bias.

We validate this bias-centric interpretation through FP4 (W4A4G4) training experiments on 1B-scale models. Mean removal narrows the loss gap relative to BF16 training and restores downstream task performance, demonstrating a hardware-efficient path to stable low-bit LLM training.

Contributions.

1. We identify coherent activation mean bias as the dominant structural component of spectral anisotropy in LLM training.
2. We show theoretically and empirically that mean bias accounts for the majority of extreme activation magnitudes that determine low-bit quantization scale.
3. We propose a source-level mean-residual splitting method that is computationally efficient and hardware-friendly.
4. We demonstrate stable FP4 (W4A4G4) training, narrowing the loss gap to BF16 and recovering downstream performance.

2 MEAN BIAS PHENOMENON

Let $\mathcal{X} \in \mathbb{R}^{b \times s \times m}$ denote an activation tensor, where b is batch size, s is sequence length, and m is hidden dimension. For GeMM analysis, reshape it into $\mathbf{X} \in \mathbb{R}^{l \times m}$ with $l = bs$, and write its SVD as

$$\mathbf{X} = \sum_{i=1}^r \sigma_i \mathbf{u}_i \mathbf{v}_i^\top, \quad r = \min(l, m), \quad \sigma_1 \geq \sigma_2 \geq \dots \geq \sigma_r > 0.$$

Define the column-wise mean vector and induced mean matrix by

$$\mu_{\mathbf{X}}^\top = \frac{1}{l} \mathbf{1}^\top \mathbf{X} \in \mathbb{R}^{1 \times m}, \quad \mathbf{M}_{\mathbf{X}} = \mathbf{1} \mu_{\mathbf{X}}^\top \in \mathbb{R}^{l \times m}.$$

We call this phenomenon *mean bias* when token representations are shifted in a common directional sense. Concretely, with normalized mean direction $\hat{\mu} = \mu_{\mathbf{X}} / \|\mu_{\mathbf{X}}\|_2$ and token rows x_i of \mathbf{X} , define $p_i = x_i^\top \hat{\mu}$. Across activation matrices in trained LLMs, the signs of $\{p_i\}$ are consistently concentrated on one side, indicating a coherent directional shift rather than symmetric fluctuation around zero. Figure 1 (left) provides one representative example from late-stage Qwen3-0.6B (layer-27 FFN input), where token-wise projection signs are nearly uniform.

We further find that the mean direction nearly recovers the leading anisotropic spike direction, which METIS identifies as the primary contributor to quantization error. Since

$$\mu_{\mathbf{X}} = \frac{1}{l} \mathbf{X}^\top \mathbf{1} = \frac{1}{l} (\mathbf{U} \Sigma \mathbf{V}^\top)^\top \mathbf{1} = \frac{1}{l} \mathbf{V} \Sigma \mathbf{U}^\top \mathbf{1},$$

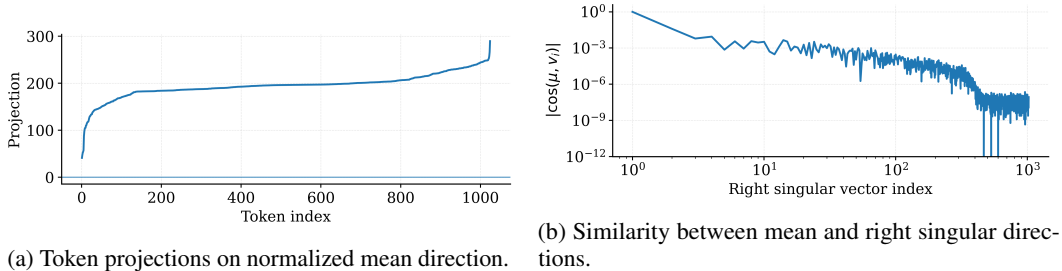


Figure 1: Evidence for mean-bias coherence and spectral dominance. Left: projection-sign consistency across tokens. Right: dominant alignment of mean vector with the top right singular vector.

we have the right-singular expansion

$$\mu_{\mathbf{X}} = \mathbf{V}\alpha = \sum_{i=1}^r \alpha_i \mathbf{v}_i, \quad \alpha_i = \frac{\sigma_i}{l} \mathbf{u}_i^\top \mathbf{1}.$$

Therefore, alignment with \mathbf{v}_1 is large when two conditions hold jointly: (i) anisotropic spectrum with dominant σ_1 , empirically observed in METIS (Cao et al., 2025), and (ii) limited sign cancellation in $\mathbf{u}_1^\top \mathbf{1}$ so that $|\alpha_1|$ remains large. In contrast, non-leading modes typically exhibit stronger sign alternation, making $\mathbf{u}_i^\top \mathbf{1}$ small and suppressing α_i for $i > 1$. Consequently, $\mu_{\mathbf{X}}$ aligns much more strongly with \mathbf{v}_1 than with other right singular directions; empirically, this cosine similarity approaches 0.99 (Figure 1, right).

3 STRUCTURAL EMERGENCE OF MEAN BIAS

We first establish the global empirical pattern of *mean bias* and then explain its mechanism. Here, mean bias refers to a coherent, nonzero feature-wise mean component that increasingly dominates activation energy across layers and training stages. This motivates a three-stage causal account: frequency-weighted initialization, nonlinear regeneration/amplification, and residual accumulation.

Empirical Trajectory: Mean-Bias Energy Rises with Training and Depth. We quantify mean magnitude by the normalized ratio

$$R = \frac{\|\mu\|_2}{\sqrt{\mathbb{E}\|X\|^2/N}}. \quad (1)$$

Using intermediate activation matrices from Qwen3-0.6B at early (10k) and late (170k) checkpoints, we decompose activations into mean + spike + tail components and track mean-energy share across embedding, shallow, middle, and deep layers. Figure 2 shows a clear trend: shallow layers already exhibit strong mean dominance early, while deep layers become increasingly mean-dominated later; in all profiled layers, mean-bias energy increases over training.

Mechanism: A Three-Stage Causal Chain. *Stage I: Statistical Origin via Frequency-Weighted Embedding Expectation.* A seed bias appears at the input representation level. Let \mathcal{V} denote vocabulary and $p(v)$ token frequency. The corpus-level expected embedding is

$$\mu_{\text{embed}} = \mathbb{E}_{v \sim p}[E_v] = \sum_{v \in \mathcal{V}} p(v) E_v, \quad (2)$$

where $E_v \in \mathbb{R}^H$ is the embedding of token v Mikolov et al. (2013b); Arora et al. (2017). Because $p(v)$ is highly non-uniform (Zipf-like), high-frequency tokens receive disproportionate updates and induce coherent embedding alignment, forming a nontrivial mean component before deeper processing.

Stage II: Nonlinear Regeneration and Amplification in Attention/FFN. Even when pre-activation features are centered, non-odd nonlinearities regenerate a nonzero mean. For a symmetric zero-mean random variable z , non-odd activations satisfy

$$\mathbb{E}[\phi(z)] > 0, \quad (3)$$

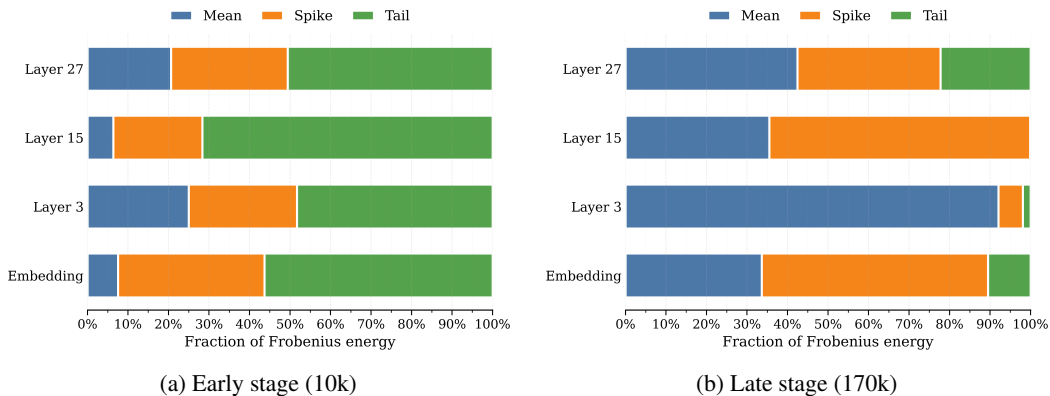


Figure 2: Mean-bias energy decomposition across layers and training stages, shown as compact summaries for early (10k) and late (170k) checkpoints.

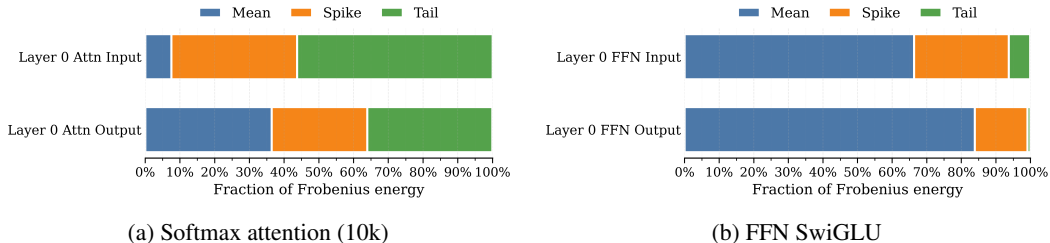


Figure 3: Operator-level input/output energy comparison. Left: attention softmax at 10k. Right: FFN SwiGLU. Both operators increase mean-bias energy from input to output.

which holds exactly for ReLU and approximately for GELU/SwiGLU due to asymmetric suppression of negative responses. In parallel, softmax attention favors coherent high-similarity directions through exponential reweighting, increasing mass on already aligned components. Empirically, operator-level input/output comparisons (Figure 3) show a consistent mean-energy increase after nonlinear processing: at 10k steps, attention softmax strengthens mean dominance; in the FFN path, SwiGLU further amplifies this effect.

Stage III: Residual Preservation and Network-Wide Accumulation. Residual connections preserve and propagate coherent mean components across depth:

$$\mu_{l+1} = \mu_l + \Delta\mu_l, \quad (4)$$

where $\Delta\mu_l$ is the layer-induced mean shift. This additive pathway prevents cancellation of existing bias and enables cumulative growth through the network. In high dimensions, even modest coordinate-wise drift becomes large in norm:

$$\|\mu\|_2 \sim \sqrt{H} \bar{\mu}, \quad (5)$$

with hidden size H Tropp (2012); Halko et al. (2011). This geometric scaling explains why mean-dominated components contribute disproportionately to extreme activations and quantization-sensitive outliers.

4 MEAN BIAS AS THE DOMINANT SOURCE OF ACTIVATION OUTLIERS

We now address its sharp structural consequence: the production of extreme elementwise activations that destabilize low-bit quantization. Because the dynamic range of low-bit quantization is strictly governed by entrywise maxima (the L_∞ norm), we perform an elementwise mechanical decomposition to precisely locate the geometric source of this instability.

Following the notation in previous sections, let the activation matrix be $X \in \mathbb{R}^{l \times m}$ with $l = bs$ token positions and hidden dimension m . To attribute outlier energy, we decompose X into three

mutually orthogonal components. Let $\mu = \frac{1}{l}X^\top \mathbf{1} \in \mathbb{R}^m$ be the feature-wise mean vector, and let $\tilde{X} = X - \mathbf{1}\mu^\top$ be the column-centered activation matrix. We decompose X as:

$$X = \underbrace{\mathbf{1}\mu^\top}_{M(\text{mean})} + \underbrace{U_k \Sigma_k V_k^\top}_{X_{\text{spike}}} + \underbrace{X_{\text{tail}}}_{\text{residual}}, \quad (6)$$

where X_{spike} is the truncated rank- k singular value decomposition of the centered matrix \tilde{X} onto its top $k = \lfloor 0.01m \rfloor$ singular directions, and $X_{\text{tail}} = \tilde{X} - X_{\text{spike}}$ is the remaining orthogonal residual. Because X_{spike} and X_{tail} are linear projections of the centered matrix, they maintain zero column means (i.e., they are orthogonal to the all-ones vector $\mathbf{1}$). Therefore, the decomposition is strictly orthogonal in the Frobenius inner product, yielding exact energy separation:

$$\|X\|_F^2 = \|M\|_F^2 + \|X_{\text{spike}}\|_F^2 + \|X_{\text{tail}}\|_F^2. \quad (7)$$

Outlier Attribution. Define the outlier set \mathcal{E}_{top} as the indices (i, j) of the top 0.1% of entries ranked by absolute magnitude $|X_{ij}|$. To determine which geometric component drives these extreme values, we define the squared-magnitude share for each $(i, j) \in \mathcal{E}_{\text{top}}$:

$$\rho_{ij}^{(\text{mean})} = \frac{M_{ij}^2}{X_{ij}^2}, \quad \rho_{ij}^{(\text{spike})} = \frac{(X_{\text{spike}})_{ij}^2}{X_{ij}^2}, \quad \rho_{ij}^{(\text{tail})} = \frac{(X_{\text{tail}})_{ij}^2}{X_{ij}^2}. \quad (8)$$

While the decomposition is strictly orthogonal over the full matrix, individual elementwise squares technically contain minor cross-terms (e.g., $2M_{ij}(X_{\text{spike}})_{ij}$). Nevertheless, measuring these primary component ratios provides a highly accurate and stable proxy for identifying the dominant driver of extreme values.

Figures 2 and 4 summarize these statistics across layers and training stages. Figure 4 shows a clear row-wise pattern: in each module (embedding, layer 3, layer 15, and layer 27), the late-stage panel (170k, right) exhibits a larger mean-component contribution to top-0.1% outliers than the corresponding early-stage panel (10k, left). In shallow modules, mean bias is already dominant at 10k and becomes near-total at 170k. In deeper modules, the 10k regime still shows stronger spike influence, but by 170k the mean term overtakes and becomes the primary outlier source. This late-stage transition to mean-dominated outliers across all four rows is the key empirical result of this section.

High-Dimensional Extreme-Value Amplification. We now formalize the statistical mechanism by which a coherent rank-one mean bias produces the dominant extreme activations observed in large language models. Our analysis proceeds in three steps. First, we show that once a deterministic mean shift exceeds the quantization threshold, individual coordinates exceed that threshold with constant probability (Theorem 1). Second, we demonstrate that this effect aggregates across tokens: a mean shift generates a dense population of extreme activations, whereas purely variance-driven fluctuations produce only exponentially rare outliers (Theorem 2). Finally, we characterize the high-dimensional scaling with a sharper lower bound: under Gaussian noise, the maximum activation in a mean-shifted coordinate is lower bounded by an additive form $|\mu_j| + (\text{extreme-value term})$, while variance-only maxima remain on the $\sigma\sqrt{\log l}$ scale (Theorem 3). Together, these results establish a fundamental asymmetry between deterministic bias and stochastic variance: a coherent mean component can systematically generate the largest elementwise activations and therefore dominate the dynamic range that governs low-bit quantization.

Theorem 1 (Elementwise Extreme Dominance). *Let an activation coordinate be modeled as*

$$X_{ij} = \mu_j + Z_{ij},$$

where μ_j is a deterministic mean shift and Z_{ij} is independent zero-mean sub-Gaussian noise with variance proxy σ^2 . For a quantization threshold $t > 0$ such that $t < |\mu_j|$, the probability that the coordinate magnitude exceeds the threshold satisfies

$$\mathbb{P}(|X_{ij}| > t) \geq 1 - 2 \exp\left(-\frac{(|\mu_j| - t)^2}{2\sigma^2}\right). \quad (9)$$

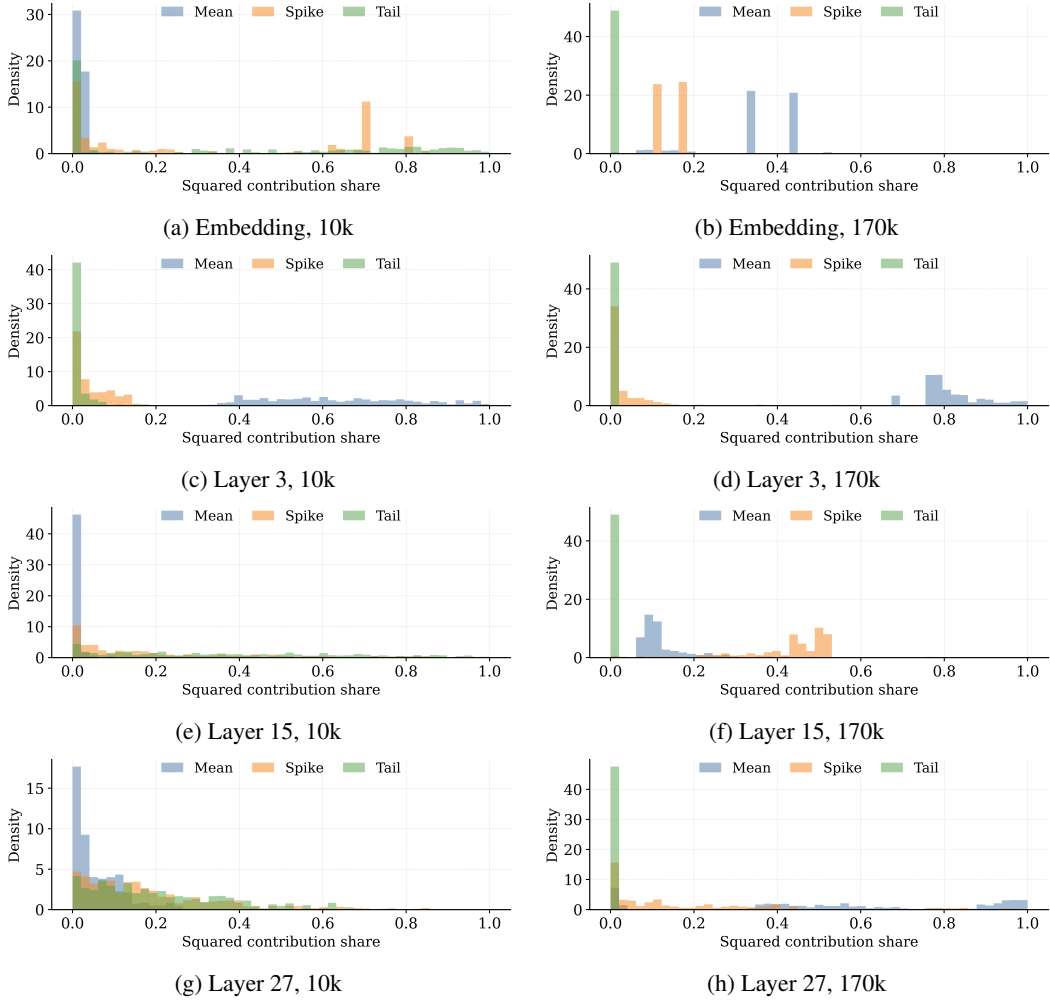


Figure 4: Activation outlier contribution shares (top 0.1% entries) across layers and training steps. Each row compares early (10k, left) and late (170k, right) for the same module.

Proof. Deferred to Appendix A.

Theorem 1 shows that once the deterministic mean shift exceeds the quantization threshold, extreme values occur with constant probability. In contrast, purely variance-driven activations $X'_{ij} = Z_{ij}$ satisfy

$$\mathbb{P}(|Z_{ij}| > t) \leq 2 \exp\left(-\frac{t^2}{2\sigma^2}\right), \quad (10)$$

which decays exponentially with the threshold.

However, the practical impact of mean bias in large models arises not only from the probability of individual extremes but from the number of such extremes produced across tokens. The following result formalizes this distinction.

Theorem 2 (Dense Extreme Amplification by Mean Bias). *Let $X_{ij} = \mu_j + Z_{ij}$ where Z_{ij} are independent mean-zero σ^2 -sub-Gaussian variables. Define the exceedance count*

$$C_j(t) = \sum_{i=1}^l \mathbf{1}\{|X_{ij}| > t\}.$$

Then:

(Mean-dominated regime) If $|\mu_j| > t$, then

$$\mathbb{E}[C_j(t)] \geq l \left(1 - 2 \exp\left(-\frac{(|\mu_j| - t)^2}{2\sigma^2}\right) \right).$$

(Variance-only regime) If $\mu_j = 0$, then

$$\mathbb{E}[C_j(t)] \leq 2l \exp\left(-\frac{t^2}{2\sigma^2}\right).$$

Thus a deterministic mean shift produces $\Theta(l)$ threshold exceedances, whereas variance-driven extremes occur only with exponentially small frequency.

Proof. Write $C_j(t) = \sum_{i=1}^l I_i$ with $I_i = \mathbf{1}\{|X_{ij}| > t\}$. By linearity of expectation,

$$\mathbb{E}[C_j(t)] = \sum_{i=1}^l \mathbb{E}[I_i] = l \mathbb{P}(|X_{ij}| > t).$$

If $|\mu_j| > t$, apply Theorem 1 to obtain

$$\mathbb{P}(|X_{ij}| > t) \geq 1 - 2 \exp\left(-\frac{(|\mu_j| - t)^2}{2\sigma^2}\right),$$

which gives the first bound. If $\mu_j = 0$, then $X_{ij} = Z_{ij}$ and sub-Gaussian tails give

$$\mathbb{P}(|X_{ij}| > t) = \mathbb{P}(|Z_{ij}| > t) \leq 2 \exp\left(-\frac{t^2}{2\sigma^2}\right),$$

yielding the second bound. □

Theorem 2 reveals a fundamental structural asymmetry. A coherent mean shift generates a *dense population of extreme activations* across tokens, whereas variance-driven fluctuations produce only sparse outliers.

Because blockwise low-bit quantization determines its dynamic range from the L_∞ norm within each block, the presence of many large-magnitude activations forces the quantization grid to expand. This expansion compresses the dynamic resolution available for the remaining semantic variation.

Consequently, even when other low-rank spike components exist, removing the coherent mean bias directly targets the primary geometric driver of extreme-value instability and restores effective numerical resolution for the semantic signal.

Theorem 3 (High-Dimensional Extreme-Value Separation (Sharper Lower Bound)). *Let activation coordinates follow*

$$X_{ij} = \mu_j + Z_{ij},$$

where $Z_{ij} \stackrel{\text{i.i.d.}}{\sim} \mathcal{N}(0, \sigma^2)$ across i . Define

$$M_j = \max_{1 \leq i \leq l} |X_{ij}|.$$

For any $\delta \in (0, 1)$, let

$$q_{l,\delta} := \sigma \Phi^{-1}((1 - \delta)^{1/l}),$$

where Φ is the standard normal CDF. Then

$$\mathbb{P}(M_j \geq |\mu_j| + q_{l,\delta}) \geq 1 - \delta.$$

In particular,

$$\mathbb{P}(M_j \geq |\mu_j|) = 1 - 2^{-l}.$$

Furthermore, in the variance-only case ($\mu_j = 0$), with probability at least $1 - \delta$,

$$\max_{1 \leq i \leq l} |Z_{ij}| \leq \sigma \sqrt{2 \log \frac{2l}{\delta}}.$$

Therefore, mean-shifted maxima enjoy an additive lower shift $|\mu_j|$ plus an extreme-value term, while variance-only maxima remain at the $\sigma \sqrt{\log l}$ scale.

Proof. Let $s_j = \text{sign}(\mu_j)$ for $\mu_j \neq 0$ (either sign can be used when $\mu_j = 0$), and define $Y_i := s_j Z_{ij}$. Since Gaussian noise is symmetric, $Y_i \stackrel{\text{i.i.d.}}{\sim} \mathcal{N}(0, \sigma^2)$. For every i ,

$$|\mu_j + Z_{ij}| \geq s_j(\mu_j + Z_{ij}) = |\mu_j| + Y_i,$$

so

$$M_j \geq |\mu_j| + \max_{1 \leq i \leq l} Y_i.$$

Hence

$$\mathbb{P}(M_j < |\mu_j| + t) \leq \mathbb{P}\left(\max_{1 \leq i \leq l} Y_i < t\right) = \Phi(t/\sigma)^l.$$

Choosing $t = q_{l,\delta}$ gives $\Phi(t/\sigma)^l = 1 - \delta$, so

$$\mathbb{P}(M_j \geq |\mu_j| + q_{l,\delta}) \geq 1 - \delta.$$

Setting $t = 0$ yields

$$\mathbb{P}(M_j \geq |\mu_j|) \geq 1 - \mathbb{P}(Y_1 < 0, \dots, Y_l < 0) = 1 - 2^{-l},$$

and equality holds because $\mathbb{P}(Y_i < 0) = 1/2$ for Gaussian noise.

For $\mu_j = 0$, the variance-only upper bound follows from the standard union bound with Gaussian (hence sub-Gaussian) tails:

$$\mathbb{P}\left(\max_{1 \leq i \leq l} |Z_{ij}| \geq u\right) \leq 2l \exp\left(-\frac{u^2}{2\sigma^2}\right),$$

then set $u = \sigma \sqrt{2 \log \frac{2l}{\delta}}$. □

Theorem 3 highlights a fundamental scaling asymmetry between coherent bias and stochastic noise. Extreme values generated by sub-Gaussian fluctuations grow only logarithmically with the number of samples, scaling as $\sigma \sqrt{\log l}$.

In contrast, coherent mean shifts accumulate systematically across layers and can scale with the representation dimension. In high-dimensional Transformer models where hidden dimension m is large, even modest coordinate-wise bias can produce magnitudes significantly exceeding the stochastic extreme-value scale.

This separation implies that once a coherent mean component forms in representation space, it naturally dominates the largest elementwise activations and therefore determines the dynamic range of low-bit quantization.

5 MEAN BIAS-AWARE LOW-BIT TRAINING METHOD

Low-bit training amplifies the pathological effects of anisotropy. Under blockwise quantization, scale is determined by extreme elementwise values. As shown in Section 4, these extremes are predominantly mean-dominated. This suggests that addressing mean bias at its source may substitute for heavier spectral corrections.

We test the following hypothesis:

If mean bias is the dominant driver of outliers, then source-level mean removal should recover most of the stability benefits attributed to SVD-based spike suppression methods such as Metis.

We propose a simple *mean-residual quantization* method, which we call *Averis* (Averaging-Induced Residual Splitting). The method targets a concrete empirical observation: for large activation-like matrices in Transformer training, extreme values (which dominate blockwise quantization scales) are largely driven by a mean-dominated component that is coherent across tokens. Accordingly, we explicitly split out a column-mean component via averaging and quantize it separately from the remaining residual, using only reduction operations and standard quantization kernels.

Notation and quantization operator. Let $\mathcal{Q}_b(\cdot)$ denote a b -bit quantization operator (e.g., block-wise FP4) applied to a matrix. We write $\bar{\mathbf{M}} \triangleq \mathcal{Q}_b(\mathbf{M})$ for the quantized version of any matrix \mathbf{M} . Throughout, $\mathbf{1}$ denotes an all-ones vector with the appropriate dimension.

Forward pass: activation mean-residual splitting. Let $\mathbf{W} \in \mathbb{R}^{m \times n}$ be a weight matrix and let $\mathcal{X} \in \mathbb{R}^{b \times s \times m}$ be an input activation tensor, where b is batch size, s is sequence length, and m is hidden dimension. As usual, we reshape \mathcal{X} into a matrix $\mathbf{X} \in \mathbb{R}^{l \times m}$ with $l = b \cdot s$ and compute the GeMM output

$$\mathbf{Y} = \mathbf{X}\mathbf{W} \in \mathbb{R}^{l \times n}.$$

We define the *activation column-mean vector* $\mu_{\mathbf{X}} \in \mathbb{R}^m$ by

$$\mu_{\mathbf{X}} \triangleq \frac{1}{l} \mathbf{1}^\top \mathbf{X},$$

The residual is

$$\mathbf{X}_{\text{R}} \triangleq \mathbf{X} - \mathbf{1} \mu_{\mathbf{X}}.$$

We then quantize the mean vector and residual independently:

$$\bar{\mu}_{\mathbf{X}} = \mathcal{Q}_b(\mu_{\mathbf{X}}), \quad \bar{\mathbf{X}}_{\text{R}} = \mathcal{Q}_b(\mathbf{X}_{\text{R}}), \quad \bar{\mathbf{W}} = \mathcal{Q}_b(\mathbf{W}).$$

The quantized forward computation is

$$\hat{\mathbf{Y}} = \mathbf{1} (\bar{\mu}_{\mathbf{X}} \bar{\mathbf{W}}) + \bar{\mathbf{X}}_{\text{R}} \bar{\mathbf{W}}. \quad (11)$$

where the first term is broadcast along the token dimension via $\mathbf{1}$. In practice, one computes $\mu_{\mathbf{X}}$ first, subtracts it from \mathbf{X} on the fly to form \mathbf{X}_{R} , and never materializes the mean matrix.

Backward pass: output-gradient mean-residual splitting. Let $\mathbf{D} \in \mathbb{R}^{l \times n}$ denote the matrix of loss derivatives with respect to the GeMM output \mathbf{Y} , i.e.,

$$\mathbf{D} \triangleq \frac{\partial \mathcal{L}}{\partial \mathbf{Y}} \quad (\text{after reshaping}).$$

We define the *output-gradient column-mean vector* $\mu_{\mathbf{D}} \in \mathbb{R}^n$ by

$$\mu_{\mathbf{D}} \triangleq \frac{1}{l} \mathbf{1}^\top \mathbf{D}, \quad \mathbf{D}_{\text{R}} \triangleq \mathbf{D} - \mathbf{1} \mu_{\mathbf{D}}.$$

Quantize the components independently:

$$\bar{\mu}_{\mathbf{D}} = \mathcal{Q}_b(\mu_{\mathbf{D}}), \quad \bar{\mathbf{D}}_{\text{R}} = \mathcal{Q}_b(\mathbf{D}_{\text{R}}).$$

Then the key GeMMs in backpropagation are evaluated as

$$\frac{\widehat{\partial \mathcal{L}}}{\widehat{\partial \mathbf{X}}} = \mathbf{1} (\bar{\mu}_{\mathbf{D}} \bar{\mathbf{W}}^\top) + \bar{\mathbf{D}}_{\text{R}} \bar{\mathbf{W}}^\top, \quad \frac{\widehat{\partial \mathcal{L}}}{\widehat{\partial \mathbf{W}}} = \bar{\mathbf{X}}_{\text{R}}^\top \bar{\mathbf{D}}_{\text{R}} + \bar{\mathbf{X}}_{\text{R}}^\top (\mathbf{1} \bar{\mu}_{\mathbf{D}}) + (\mathbf{1} \bar{\mu}_{\mathbf{X}})^\top \bar{\mathbf{D}}_{\text{R}} + (\mathbf{1} \bar{\mu}_{\mathbf{X}})^\top (\mathbf{1} \bar{\mu}_{\mathbf{D}}). \quad (12)$$

The additive terms are accumulated with broadcasted additions without explicitly storing $\mathbf{M}_{\mathbf{X}}$ or $\mathbf{M}_{\mathbf{D}}$.

Computational profile. Averis requires only computing two mean vectors ($\mu_{\mathbf{X}}$ and $\mu_{\mathbf{D}}$) and applying two subtractions per step, in addition to the baseline quantized GeMMs. No spectral decomposition or iterative orthogonalization is involved, and all additional operations are GPU-friendly reductions and elementwise kernels.

6 MEAN BIAS-AWARE LOW-BIT TRAINING EXPERIMENTS

6.1 EXPERIMENTAL SETUP

Models and Datasets. We conduct experiments on Qwen-3 (0.6B). For pretraining, we use the DCLM dataset and train the model on 100B tokens. The raw data are segmented to split long documents and concatenate short ones, filtered to remove non-Unicode and non-English content.

FP4 Training. We evaluate the efficacy of Averis under FP4 quantization against BF16 baselines. All FP4 training in this work adopts W4A4G4 quantization, where weights, activations, and gradients are represented in the E2M1 NVFP4 format. Stochastic rounding (SR) is applied by default in all FP4 experiments, as it mitigates quantization bias and is orthogonal to Averis.

Baselines. We compare the following settings:

- **BF16:** full-precision baseline.
- **Vanilla FP4:** direct NVFP4 quantization (W4A4G4) without structural splitting.
- **Averis FP4:** the proposed mean-residual splitting applied to activations and output gradients, with independent quantization of mean vectors and residuals.

6.2 RESULTS

Training loss. Figure 5 shows the training loss curves of the BF16 baseline and FP4 + Averis. Averis remains slightly above BF16 in loss, while clearly improving over vanilla FP4.

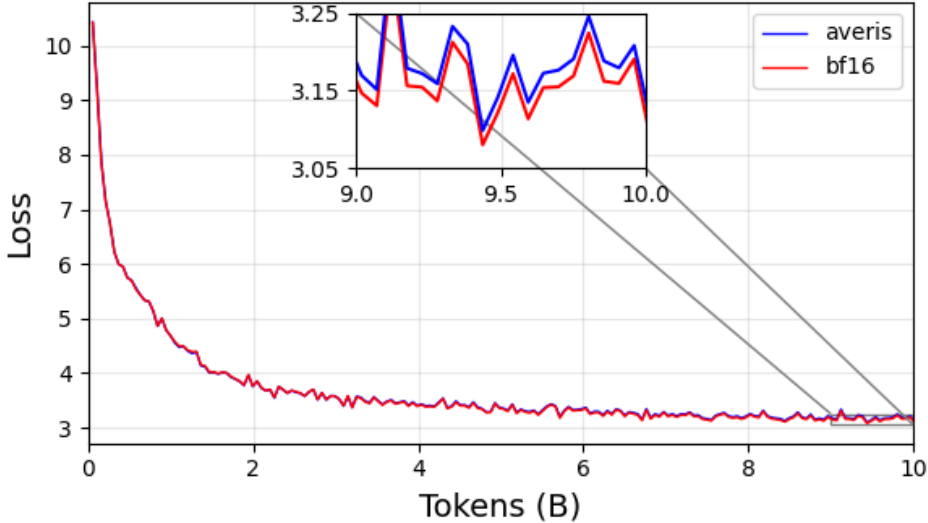


Figure 5: Training loss curves for Qwen3-0.6B under BF16 and FP4 + Averis.

Downstream performance at 10B tokens. At the 10B-token checkpoint, we evaluate BF16 and Averis on seven downstream tasks. As shown in Table 1, Averis improves the average score from 0.4564 to 0.4661.

Table 1: Downstream task results at 10B tokens.

Method	ARC-C	ARC-E	BoolQ	HellaSwag	LAMBADA	PIQA	RACE	Avg
BF16	0.2534	0.5126	0.5309	0.3768	0.3602	0.6730	0.4882	0.4564
Averis	0.2491	0.5072	0.5746	0.3751	0.3862	0.6670	0.5036	0.4661

7 RELATED WORK

7.1 ANISOTROPY IN REPRESENTATION GEOMETRY

Anisotropy in learned representations has been widely observed in both static and contextual embedding models. Ethayarajh Ethayarajh (2019) showed that contextualized representations from BERT, ELMo, and GPT-2 occupy a narrow cone in representation space, exhibiting strong directional concentration. Mu and Viswanath Mu & Viswanath (2018); Mu et al. (2017) demonstrated that removing

the top principal components from word embeddings significantly improves isotropy and downstream semantic similarity. Arora et al. (2017) similarly proposed subtracting a common discourse vector in sentence embeddings to mitigate dominant shared components. Subsequent analyses identified “rogue dimensions” and dominant outlier directions in Transformer models Timkey & van Schijndel (2021); Kovaleva et al. (2021), while more recent work argued that anisotropy may depend on training conditions rather than being inherent to Transformer architecture Machina et al. (2024).

These studies establish anisotropy as a persistent geometric phenomenon. However, they primarily treat it as a spectral artifact to be post-processed or regularized. In contrast, our work identifies a specific structural source of anisotropy: a coherent activation mean bias originating from the embedding layer, which propagates through residual connections and dominates elementwise extremes during training.

7.2 FREQUENCY EFFECTS AND EMBEDDING STRUCTURE

The relationship between word frequency and embedding geometry has been recognized since early distributed representation models. Word2Vec Mikolov et al. (2013a;b) introduced subsampling of frequent tokens to reduce dominance of high-frequency words during training. Arora et al. (2017) provided a generative model explaining why common words induce a shared background direction in embeddings. Mu and Viswanath (2018) formalized the removal of dominant principal components to restore isotropy. More recently, Puccetti et al. (2022) argued that outlier dimensions in Transformers are driven by token frequency.

While prior work links frequency to dominant directions, it largely focuses on representational quality. We extend this perspective to training dynamics, showing that frequency-induced embedding bias becomes the dominant driver of activation outliers and optimizer second-moment inflation, with direct implications for large-scale training stability.

7.3 OUTLIER SUPPRESSION AND LOW-BIT QUANTIZATION

Outlier dimensions and extreme activation magnitudes have been a central challenge in low-bit quantization of large language models. SmoothQuant Xiao et al. (2023) redistributes activation and weight scales to reduce outlier concentration. GPTQ Frantar et al. (2023), AWQ Lin et al. (2024), QLoRA Dettmers et al. (2023), and SVDQuant Li et al. (2024) propose various strategies to absorb or compensate for large-magnitude components. QuaRot Ashkboos et al. (2024) and HALO Ashkboos et al. (2025) employ orthogonal rotations or Hadamard transforms to mitigate outliers. Outlier Suppression Wei et al. (2023) explicitly targets extreme activation dimensions. Recent work on FP8 and FP4 training further highlights the sensitivity of low-precision regimes to activation dynamic range Micikevicius et al. (2022); Peng et al. (2023); Perez et al. (2023); Cao et al. (2025).

These methods typically treat outliers as spectral imbalances requiring rotation, clipping, or decomposition. Our analysis shows that a large fraction of extreme activation magnitudes is attributable to a rank-one mean bias component. Addressing this bias at the embedding activation level significantly reduces dynamic-range inflation before more complex spectral corrections are applied.

7.4 EFFICIENT SPECTRAL APPROXIMATION AND WHITENING

Low-rank approximation and spectral methods are classical tools for controlling anisotropy. Randomized SVD Halko et al. (2011) and distributed low-rank algorithms Suresh et al. (2017) provide scalable approximations of dominant singular directions. Oja’s rule Oja (1982) and whitening-based approaches Huang et al. (2021) offer incremental spectral normalization.

However, applying SVD or whitening repeatedly across large models remains computationally expensive. Our work shows that a significant portion of harmful anisotropy is concentrated in a coherent rank-one bias component, allowing a single mean-subtraction operation to achieve much of the desired conditioning effect at minimal cost. Residual low-rank whitening can then be applied selectively at the embedding activation level rather than throughout the network.

Positioning. Prior work has identified anisotropy, frequency-driven dominant directions, and outlier suppression strategies. We synthesize these threads by demonstrating that mean-dominated activation

bias constitutes a primary structural source of anisotropy in large language model training. By tracing this bias to embedding frequency statistics and quantifying its impact on both quantization and optimization, we provide a unified perspective that connects representation geometry, training stability, and hardware efficiency.

8 CONCLUSION

We revisited anisotropy in large language model training and identified a sharper structural principle: *activation anisotropy is predominantly driven by a coherent rank-one mean bias*. This mean component arises naturally from hierarchical semantic aggregation and accumulates through residual pathways, systematically regenerating coherent directions in representation space.

In high-dimensional settings, even modest coordinate-wise bias scales as $\|\mu\|_2 \sim \sqrt{H} \bar{\mu}$, amplifying small drift into dominant elementwise extremes. Because blockwise low-bit quantization scales are determined by these extremes, mean bias becomes the principal driver of dynamic-range inflation and numerical instability. We show that this dominant rank-one component can be removed through a simple source-level mean subtraction, providing effective spectral conditioning using only reduction and elementwise operations.

These findings recast anisotropy as both a *curse* and a *blessing*: the same structured mean bias that destabilizes low-bit training also exposes a low-dimensional handle for efficient mitigation. By isolating and removing this component at its source, we obtain a hardware-friendly path to stable low-bit LLM training.

REFERENCES

- Sanjeev Arora, Yingyu Liang, and Tengyu Ma. A simple but tough-to-beat baseline for sentence embeddings. In *International Conference on Learning Representations (ICLR)*, 2017. URL <https://openreview.net/forum?id=SyK00v5xx>.
- Saleh Ashkboos et al. Quarot: Outlier-free 4-bit inference in rotated llms. In *NeurIPS*, 2024.
- Saleh Ashkboos et al. Halo: Hadamard-assisted lower-precision optimization. arXiv:2501.02625, 2025.
- Hengjie Cao, Mengyi Chen, Yifeng Yang, Ruijun Huang, Fang Dong, Jixian Zhou, Anrui Chen, Mingzhi Dong, Yujiang Wang, Jinlong Hou, Yuan Cheng, Fan Wu, Fan Yang, Tun Lu, Ning Gu, and Li Shang. Metis: Training llms with fp4 quantization. arXiv preprint arXiv:2509.00404, 2025. URL <https://arxiv.org/abs/2509.00404>.
- Tim Dettmers, Artidoro Pagnoni, Ari Holtzman, and Luke Zettlemoyer. Qlora: Efficient finetuning of quantized LLMs. In *Advances in Neural Information Processing Systems (NeurIPS)*, 2023. URL <https://arxiv.org/abs/2305.14314>.
- Kawin Ethayarajh. How contextual are contextualized word representations? comparing the geometry of BERT, ELMo, and GPT-2 embeddings. In *Proceedings of EMNLP-IJCNLP*, 2019. URL <https://aclanthology.org/D19-1006/>.
- Elias Frantar, Saleh Ashkboos, Torsten Hoefler, and Dan Alistarh. Gptq: Accurate post-training quantization for generative pre-trained transformers. In *International Conference on Learning Representations (ICLR)*, 2023. URL <https://arxiv.org/abs/2210.17323>.
- Nathan Halko, Per-Gunnar Martinsson, and Joel A. Tropp. Finding structure with randomness: Probabilistic algorithms for constructing approximate matrix decompositions. *SIAM Review*, 53(2):217–288, 2011. URL <https://arxiv.org/abs/0909.4061>.
- Junjie Huang, Duyu Tang, Wanzhu Li, Yongbin Chen, and Nan Duan. Whiteningbert: An easy unsupervised sentence embedding approach. In *Findings of EMNLP*, 2021. URL <https://aclanthology.org/2021.findings-emnlp.23/>.
- Olga Kovaleva, Saurabh Kulshreshtha, Anna Rogers, and Anna Rumshisky. BERT busters: Outlier dimensions that disrupt transformers. In *Findings of ACL-IJCNLP*, 2021. URL <https://aclanthology.org/2021.findings-acl.300/>.
- Muyang Li et al. Svdquant: Absorbing outliers by low-rank components. In *Advances in Neural Information Processing Systems (NeurIPS)*, 2024.
- Ji Lin, Jiaming Tang, et al. Awq: Activation-aware weight quantization for on-device LLM compression and acceleration. In *Proceedings of MLSys*, 2024. URL <https://arxiv.org/abs/2306.00978>.
- A. Machina et al. Anisotropy is not inherent to transformers. In *Proceedings of NAACL*, 2024. URL <https://aclanthology.org/2024.naacl-long.274/>.
- Paulius Micikevicius et al. Fp8 formats for deep learning. arXiv preprint arXiv:2209.05433, 2022.
- Tomas Mikolov, Kai Chen, Greg Corrado, and Jeffrey Dean. Efficient estimation of word representations in vector space. arXiv preprint arXiv:1301.3781, 2013a.
- Tomas Mikolov, Ilya Sutskever, Kai Chen, Greg Corrado, and Jeffrey Dean. Distributed representations of words and phrases and their compositionality. In *Advances in Neural Information Processing Systems (NeurIPS)*, 2013b.
- Jiaqi Mu and Pramod Viswanath. All-but-the-top: Simple and effective postprocessing for word representations. In *International Conference on Learning Representations (ICLR)*, 2018.
- Jiaqi Mu, Suma Bhat, and Pramod Viswanath. All-but-the-top: Simple and effective postprocessing for word representations. arXiv preprint arXiv:1702.01417, 2017. URL <https://arxiv.org/abs/1702.01417>.

-
- Erkki Oja. Simplified neuron model as a principal component analyzer. *Journal of Mathematical Biology*, 1982.
- Bo Peng et al. Fp8 quantization: The power of the exponent. arXiv preprint, 2023.
- Fabian Perez et al. Fp8 training: Scalable training with 8-bit floating point. arXiv preprint, 2023.
- Giovanni Puccetti, Anna Rogers, and Aleksandr Drozd. Outlier dimensions that disrupt transformers are driven by frequency. arXiv:2205.11380, 2022.
- Anshumali Suresh, Felix X. Yu, Sanjiv Kumar, Pradeep Ravikumar, and Inderjit S. Dhillon. A distributed and efficient method for the low-rank approximation of matrices. In *Proceedings of the 34th International Conference on Machine Learning (ICML)*, 2017. URL <https://proceedings.mlr.press/v70/suresh17a.html>.
- William Timkey and Marten van Schijndel. All bark and no bite: Rogue dimensions in transformer language models obscure representational quality. In *Proceedings of EMNLP*, 2021. URL <https://arxiv.org/abs/2109.04404>.
- Joel Tropp. User-friendly tail bounds for sums of random matrices. *Foundations of Computational Mathematics*, 2012.
- Xiuying Wei et al. Outlier suppression: Pushing the limits of low-bit large language model quantization. arXiv preprint, 2023.
- Guangxuan Xiao, Ji Lin, Wei Zhang, et al. Smoothquant: Accurate and efficient post-training quantization for large language models. In *Proceedings of ICML*, 2023. URL <https://arxiv.org/abs/2211.10438>.

A PROOF OF THEOREM 1

Let

$$X_{ij} = \mu_j + Z_{ij},$$

where Z_{ij} is mean-zero σ^2 -sub-Gaussian. For $t < |\mu_j|$, reverse triangle inequality gives

$$|X_{ij}| \geq |\mu_j| - |Z_{ij}|.$$

Hence

$$\{|Z_{ij}| < |\mu_j| - t\} \subseteq \{|X_{ij}| > t\},$$

so

$$\mathbb{P}(|X_{ij}| > t) \geq \mathbb{P}(|Z_{ij}| < |\mu_j| - t).$$

Using the sub-Gaussian tail bound

$$\mathbb{P}(|Z_{ij}| \geq u) \leq 2 \exp\left(-\frac{u^2}{2\sigma^2}\right),$$

with $u = |\mu_j| - t$ yields

$$\mathbb{P}(|X_{ij}| > t) \geq 1 - 2 \exp\left(-\frac{(|\mu_j| - t)^2}{2\sigma^2}\right).$$

This proves Theorem 1.

B PROOF OF THEOREM 2

Let

$$X_{ij} = \mu_j + Z_{ij},$$

where Z_{ij} are independent mean-zero sub-Gaussian random variables with variance proxy σ^2 .

Define the exceedance indicator

$$B_i = \mathbf{1}\{|X_{ij}| > t\},$$

and the total exceedance count

$$C_j(t) = \sum_{i=1}^N B_i.$$

B.1 MEAN-DOMINATED REGIME

Assume $|\mu_j| > t$.

By the reverse triangle inequality

$$|X_{ij}| = |\mu_j + Z_{ij}| \geq |\mu_j| - |Z_{ij}|.$$

Thus if

$$|Z_{ij}| < |\mu_j| - t,$$

then necessarily

$$|X_{ij}| > t.$$

Therefore

$$\mathbb{P}(|X_{ij}| > t) \geq \mathbb{P}(|Z_{ij}| < |\mu_j| - t).$$

Because Z_{ij} is sub-Gaussian,

$$\mathbb{P}(|Z_{ij}| \geq u) \leq 2 \exp\left(-\frac{u^2}{2\sigma^2}\right).$$

Setting $u = |\mu_j| - t$ gives

$$\mathbb{P}(|X_{ij}| > t) \geq 1 - 2 \exp\left(-\frac{(|\mu_j| - t)^2}{2\sigma^2}\right).$$

Since the indicators B_i are independent,

$$\mathbb{E}[C_j(t)] = \sum_{i=1}^N \mathbb{E}[B_i] = \sum_{i=1}^N \mathbb{P}(|X_{ij}| > t).$$

Using the lower bound above yields

$$\mathbb{E}[C_j(t)] \geq N \left(1 - 2 \exp\left(-\frac{(|\mu_j| - t)^2}{2\sigma^2}\right)\right).$$

B.2 VARIANCE-ONLY REGIME

If $\mu_j = 0$, then $X_{ij} = Z_{ij}$ and

$$\mathbb{P}(|X_{ij}| > t) = \mathbb{P}(|Z_{ij}| > t).$$

Using the sub-Gaussian tail bound

$$\mathbb{P}(|Z_{ij}| > t) \leq 2 \exp\left(-\frac{t^2}{2\sigma^2}\right),$$

we obtain

$$\mathbb{E}[C_j(t)] = \sum_{i=1}^N \mathbb{P}(|Z_{ij}| > t) \leq 2N \exp\left(-\frac{t^2}{2\sigma^2}\right).$$

B.3 INTERPRETATION

The two regimes differ fundamentally:

$$\text{Mean-dominated: } C_j(t) = \Theta(N)$$

$$\text{Variance-only: } C_j(t) = \mathcal{O}\left(N e^{-t^2/(2\sigma^2)}\right).$$

Thus a coherent mean shift produces a dense population of extreme activations across tokens, whereas purely variance-driven extremes are exponentially rare.

This scaling difference explains why mean bias becomes the dominant driver of activation outliers in large models.